ORIGINAL ARTICLE

Outdoor measurements of thoron progeny in a ^{232}Th-rich area with deposition-based alpha track detectors and corrections for wind bias

Hallvard Haanes,[1,2]* Hilde Kristin Skjerdal,[1] Rosaline Mishra[3] and Anne Liv Rudjord[1,2]

[1]Norwegian Radiation and Nuclear Safety Authority, Østerås, Norway; [2]Centre for Environmental Radioactivity (CERAD CoE), Norwegian University of Life Sciences (NMBU), Norway; [3]Bhabha Atomic Research Centre, Trombay, Mumbai, India

Abstract

Radon and thoron progeny are important contributors to dose from naturally occurring radionuclides, especially in high background areas and with naturally occurring radioactive material (NORM) legacy sites. Due to the short half-life of thoron, measurements of thoron progeny with a longer half-life should be used for risk and dose assessment. Deposition-based alpha track detectors for such progeny are, however, biased by air movement, especially outdoors where winds may be strong but variable. We used deposition detectors for thoron progeny and radon progeny, as well as alpha track gas detectors for ^{220}Rn and ^{222}Rn, outdoors within the Fen complex in Norway, an area with both elevated levels of naturally occurring radionuclides and NORM legacy sites. Different detector types were used and showed different results. We measured airflow along deposition detectors during deployment to assess wind bias and used statistical models to attain location-specific sheltering factors. These models assess how explanatory terms like point measurements with anemometer, predicted airflow along detectors, and levels of ^{220}Rn and ^{222}Rn explained variation in deposition detector measurements of TnP and RnP. For all the detector types, unrealistically, high equilibrium values (F) were found between progenitor noble gas and progeny before correcting for wind bias. Results suggest a magnitude of wind bias on TnP deposition detectors being a fraction of 0.74–0.96 (mean: 0.87) of the total measurement.

Keywords: *outdoor thoron progeny*; *outdoor thoron*; *alpha track deposition detectors*; *air movement*; *deposition wind bias*; *decommissioned mines*

Radon (^{222}Rn) and thoron (^{220}Rn) progeny (RnP and TnP) are important contributors to dose, received by the public from natural sources of radiation (1, 2), especially in high background radiation areas and with NORM legacy sites (3, 4). One such area is Fen complex in Norway (Fig. 1). Here, one type of bedrock (redrock) is especially rich in thorium (^{232}Th), involving high outdoor levels of ^{220}Rn and TnP in the sub-area Mining hill due to surficial redrock and legacy mines (5–8). Risk assessment has been based on measurements of gamma radiation, and radon and thoron concentrations (6). However, ^{220}Rn half-life is short (55 s), and measurements are uncertain and highly dependent on distance to source (1, 2, 9). Dose assessment should therefore be based on direct measurements of TnP (10–13).

^{222}Rn and ^{220}Rn progeny react very quickly (<1 s) with trace gases, water vapor, and other radionuclides to form clusters (0.5–5 nm). These clusters, which are termed unattached progeny, are mostly positively charged with high mobility, involving deposition on surfaces or attachment to aerosols (1–100 s), which are then termed attached progeny (14). Alpha track detectors for RnP and TnP are based on surface deposition, and activity concentrations are calculated after calibration against indoor deposition velocities (13, 15, 16). There is, however, an upward bias on deposition velocities from air movement (14, 17), which has been assessed and found significant for low velocities typical of indoor conditions (16, 18). Methodology to cope with velocities typical to outdoor wind bias is, however, lacking. By taking local outdoor air movement into account, variation in TnP should be even better explained by statistical modeling rather than just accounting for local levels of ^{220}Rn. We therefore recorded air movement along outdoor detectors, as well as concurrent wind conditions during TnP and RnP deposition detector deployment at localities in Mining hill (redrock part of Fen complex). First, we assess which factors that explain variation in airflow along detectors. Then, to assess wind bias, we address how airflow may explain variation in deposition of progeny while

accounting for activity concentrations of ^{220}Rn and ^{222}Rn. In doing so, we also address whether point measurements of airflow along detectors are sufficient or whether predictions of airflow based on statistical models including wind conditions are better.

Methods

Area, source description, and seasonality

Fen igneous complex (Fig. 1) is an ancient (580 mill y) eroded carbonatite volcano where magmatic and hydrothermal processes have enriched bedrock in metals and radionuclides: ^{232}Th in redrock and ankerite and ^{238}U in Søvite (8, 19–21). Deep Holocene deposits cover much of Fen complex. Also, there are two mining legacy sites: (1) Fen iron mines in Mining hill, operated mid-17th until the 20th century and (2) Søve niobium mines, operated in the mid-20th century. Within the Mining hill, there are redrock surfaces, and there is an exhalation of ^{220}Rn from soil and waste rock deposits, as well as natural ventilation of the legacy mines, leading to significant outdoor levels of ^{220}Rn and TnP (5–8, 22). The natural 'chimney' ventilation of the old Fen mines (27–42 kBq m^{-3} of ^{220}Rn) depends mostly on outside temperature and involves large releases through mine openings (22). Seasonality and diurnal variation of outside temperatures, thus, affect the direction and magnitude of Fen mines 'chimney' ventilation, which can have local impact as large as up to a GBq per day (22). In temperate countries like Norway, water freezing within the ground and snow cover can

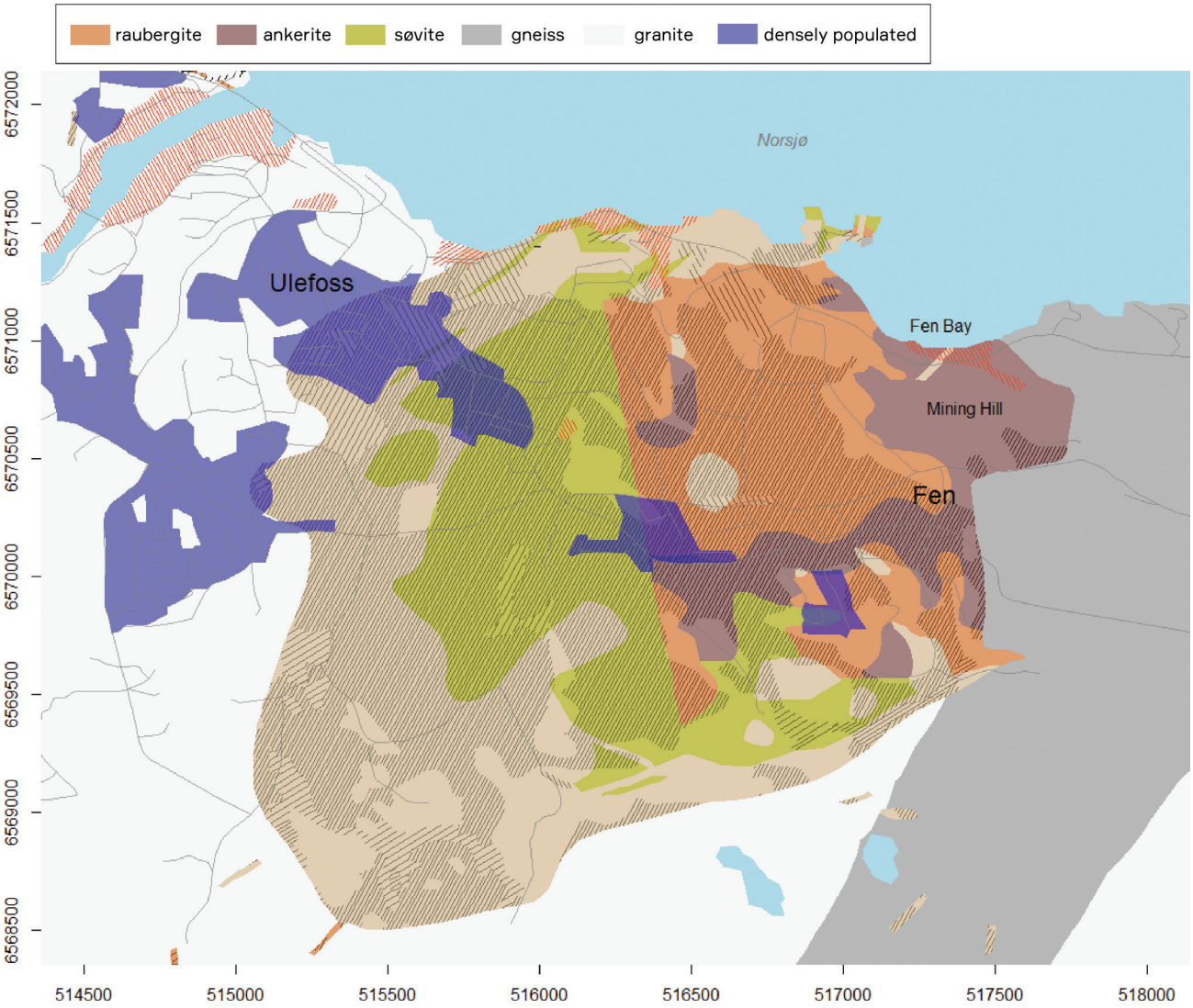

Fig. 1. Fen igneous complex with: radionuclide-enriched bedrock and densely populated areas in color (see legend), two mining legacy sites: (1) red square: Fen iron mines and (2) green square: Søve niobium mines, Holocene deposits (hatched), and anthropogenic deposits (red hatched). UTM 33 projection coordinates with WGS 84 datum on X and Y axis.

Citation: Journal of the European Radon Association 2021, **2**: 6130 http://dx.doi.org/10.35815/radon.v2.6130

heavily reduce exhalation from soil and waste rock deposits. Mining hill is characterized by many mine entrances, as well as deposits of waste rock and a shallow soil layer, and there are many well used footpaths. Characterization of spatiotemporal exposure within this forested hillside is, thus, complex.

Alpha track detector measurements

For one winter period of 64 days (2016 Jan 6 to Mar 10) and one summer period of 12 days (2018 May 31 to Jun 12), outdoor levels of TnP, RnP, ^{220}Rn, and ^{222}Rn were assessed in Mining hill. This was done at different locations (n = 25 in winter and n = 35 in summer), using a set of different time integrating alpha track detectors. Each set consisted of one open TnP deposition detector (NIRS, Japan), two pairs of TnP and RnP deposition detectors (BARC, India), where one pair is meshed and the other is open (13, 23, 24), and a ^{222}Rn and ^{220}Rn detector-pair (Radonova). TnP and RnP activity concentrations are estimated and expressed as equivalent equilibrium concentrations (EEC) of the parent gas (^{220}Rn/^{222}Rn). At each location, the detector set was placed at approximately 100 cm height beneath a sheltering roof (Fig. 2). Localities were subdivided according to subarea (hillside, bay, and ravine) and proximity to mine entrances (adjacent, close or not).

The NIRS TnP deposition detector (CR-39) was provided by Radonova, developed by the National Institute of Radiological Sciences (NIRS, Japan). It has been laboratory-calibrated under indoors conditions with known activity concentrations of TnP (15). It records alpha particles from ^{212}Po as an aluminized Mylar film that excludes contributions from other progeny with lower energy, and track densities yield estimates of equivalent equilibrium concentration of thoron (EECT) (Bq m^{-3}). The measurement uncertainties (1 SD) of this detector were in the range of 2–60%, with a median of 10%.

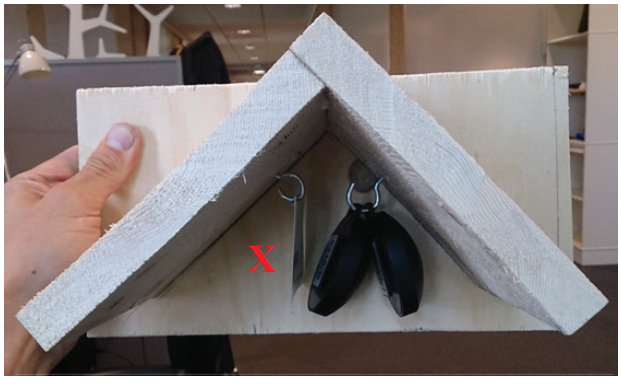

Fig. 2. Alpha track detector shelter used at each location. The TnP/RnP meshed and open detectors are not shown on photo but were mounted with clips, so that they were under the roof and in front of the back wall. Point of airflow measurement indicated by X.

The BARC RnP/TnP-type deposition detectors (LR-115) were developed and provided by Bhabha Atomic Research Centre (BARC, India). They have been laboratory calibrated under indoor conditions with known activity concentrations of TnP and RnP (13, 16, 23, 25). One BARC RnP/TnP pair consist of open detectors (equivalent to NIRS), while the other pairs are detectors covered by a fine metal mesh. On the fine mesh, the fine fraction attaches, while the coarser fraction of attached progeny passes and deposits. Track densities yield estimates of EECR and EECT. Indoor calibration has been done at 0.02 m s^{-1}, and increasing ventilation rates show an approximate linear bias on deposition velocity and sensitivity factors (16, 18). This is similar to what has been seen for vertical deposition in wind tunnels (26). We therefore calculated a parameter: the ratio between observed airflow along detectors compared to laboratory calibration conditions (i.e. how many times faster actual airflow is compared to 0.02 m s^{-1}). To account for wind bias on the BARC deposition detectors, the product of the sensitivity factor and this parameter was, thus, added to the sensitivity factor. The magnitude of wind bias was assessed with this correction, and the results were compared with the magnitude of wind bias predicted by the most likely statistical model.

The ^{222}Rn and ^{220}Rn detector pair was provided and analyzed by Landauer Nordic AB (Radtrack2 CR-39; ISO 11665-4), where one detector only allows slow diffusion of ^{222}Rn, while the other has free passage of both gases. The difference in alpha tracks is together with exposure time used to calculate the activity concentrations of the two gases. The measurement uncertainties (1 SD) had a range of 8–68% with a median of 18% for ^{222}Rn and a range of 7–34% with a median of 8% for ^{220}Rn.

Wind and measurements of air movement

Measurements of airflow were done at each location using a Kanomax climomaster 6501 anemometer using a hot-wire probe (model 6543) beneath each detector shelter (Fig. 2). Measurements were done within a couple of centimeters from the deposition detectors, in series with approximately 5 s intervals, recording the 5 s running average (m s^{-1}). The instrument measures simultaneously air movement in all directions (omnidirectional) for velocities from 0.01 to 5 m s^{-1} with an accuracy of ± 2%. Zero measurements were set to 0.001 for calculation purposes (avoiding infinity). During the summer detector deployment period in 2018, in total, 2,836 measurements were made beneath detector shelters (per shelter: 10–35, mean: 20, and SD: 4). These were made during 9, 4, 4, and 6 of the hours of four summer days. In addition, airflow measurements were made in 'free air' at 1 m height adjacent to 27 shelter locations (n = 414) on two of the four summer days to assess the sheltering effect of shelters. During the

winter detector deployment in 2016, no anemometer measurements were done. To approximate airflow along detectors during winter conditions, 915 airflow measurements were done beneath detector shelters on two winter days in winter 2017, covering 3 and 4 h.

Hourly weather data were downloaded for the two detector deployment periods from the closest weather station (St.no. = 32,060, 1,100 m to NNW, 59.380644°N, 9.201890°E). These included outside temperature (°C), precipitation (mm h^{-1}), snow depth (cm), wind speed (m s^{-1}), and direction (degrees) at 10 m height (www.eklima.no). Weather data were also downloaded for the hours of anemometer airflow measurements during the two approximative winter-days in March 2017.

Statistics

Wind strength, air movement, and the activity concentration measurements of all radionuclides had unambiguous approximate log-normal distributions when inspected in histograms. To normalize these data, airflow and wind speed were log2-transformed (+0.01 if zero present) before statistical analyses, while activity concentrations due to wide ranges and maximum values involving much longer distribution tails were log10-transformed (+0.01). We used base R for statistics (27, 28), packages sp (29) and rgdal (30) for map making, and package openair (31) for wind roses.

To assess how wind speed and direction affect airflow velocities beneath detector shelters, a linear model of variation in airflow beneath shelters ($\log_2$) was made. Wind speed ($\log_2$) and direction were included as predictor variables, as well as location identity to include possible topographical and vegetational sheltering effects. We used reverse Helmert contrasts (contrast package R), which compares each new level with the mean of previous levels. In this model, only data from the four summer deployment days were included.

The summer anemometer measurements and the approximative winter anemometer measurements were initially used directly to account for BARC detector wind bias. However, during the deployment periods, there could be variation in wind velocities, and thus in wind bias. We therefore assessed to what degree point measurements of airflow beneath detector shelters are representative for the whole deployment period. This was done by estimating an integrated measure of airflow beneath each detector shelter during each deployment period for comparison. The ratio between airflow beneath the detector shelter at each detector location and wind speed was calculated to attain location-specific factors to predict airflow along detectors from wind speed during the deployment period (multiplying wind speed with this factor). This was done for both the summer deployment period and the approximative winter measurements. These factors express location-specific sheltering effect of each detector shelter. Estimates of integrated airflow beneath each detector shelter for each whole deployment period were then estimated using average wind data during each of the deployment periods (winter and summer) and multiplying with the location-specific sheltering factors.

We wanted to assess whether point airflow measurements (the actual anemometer measurements) or the predicted integrative estimates of airflow (via location-specific sheltering factors) during the whole deployment period differ in explaining variation in progeny deposition during the deployment periods. We also wanted to assess the magnitude of wind bias. We therefore explored alternative linear statistical models for the biased (not corrected for wind bias) activity concentration of thoron/radon (EECn) measured with BARC and NIRS deposition detectors at each locality and each of the two deployment periods (Table 3). These models included either actual anemometer measurements or predicted integrative measurements of airflow, as well as measurements of progenitor gases (^{220}Rn/^{222}Rn) as predictor variables (Table 3). Depending on model results, either anemometer measurements would be taken as representative and used directly in correcting for wind bias, or the airflow predicted by the location-specific sheltering factors beneath each detector shelter from wind speed during deployment periods would be used to correct for wind bias.

Results

During detector deployment, the mean wind speed (at 10 m height) was 2 m s^{-1} (SD = 1, range: 0.1–8) in winter and 2 m s^{-1} (SD = 1, range: 0.2–6) in summer, but there was much variation both diurnally and among days (Fig. 3). The winter period had a mean temperature of minus 3°C (SD = 5), received 96 mm precipitation, had a mean snow depth of 6 cm (SD = 4), and a mean atmospheric pressure of 993 hPa (SD = 13, range: 962–1,061). The seasonality of the area was apparent from the higher and less variable temperatures of the summer deployment period (Fig. 3) with a mean of 19°C (SD = 5), no snow or ice, only 4 mm precipitation and higher and less variable atmospheric pressure with a mean of 1,002 hPa (SD = 5, range: 990–1,012). Seasonality was also apparent in the measured levels of outdoor ^{222}Rn and ^{220}Rn and their progenies (uncorrected for wind bias, Figs. 4 & 5), which can be expected due to the differences in ice cover and natural mine ventilation.

The outdoor levels of ^{222}Rn and especially ^{220}Rn were relatively high (Tables 1 & 2) and significantly higher in summer than winter (log-transformed: $t > 11$, $P < 0.001$), as well as near mine openings (Figs. 6 & 7). This pattern was reflected in the deposition detector results but with large deviations for the ravine locality between the NIRS and BARC detectors. Corresponding log-transformed

Citation: Journal of the European Radon Association 2021, **2**: 6130 http://dx.doi.org/10.35815/radon.v2.6130

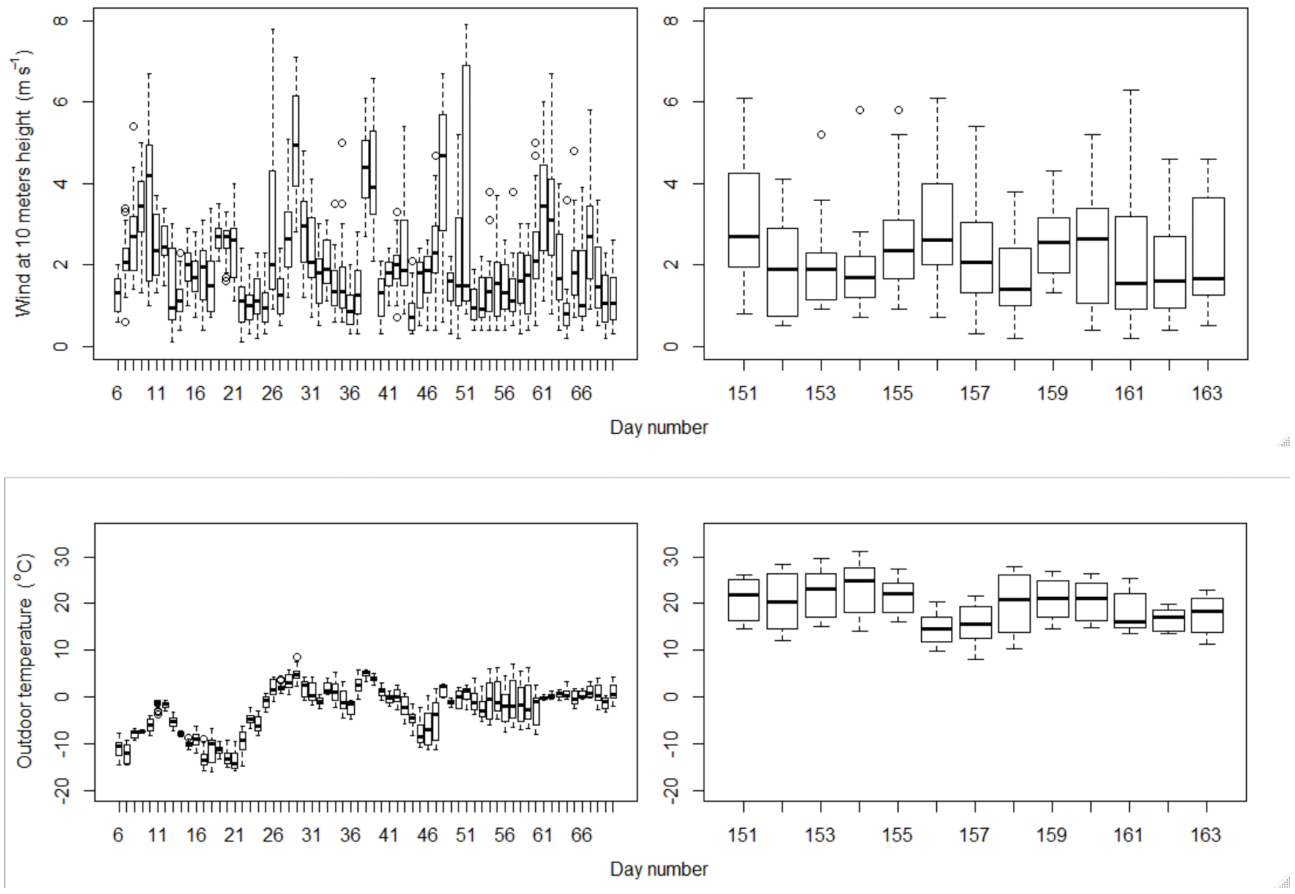

Fig. 3. Boxplots of diurnal variation in outdoor temperature (°C, 2 m height) and wind velocity (m s^{-1}, 10 m height) recorded at nearby weather station: yearly day-number from January first on x-axis, for two periods of alpha track detector deployment: January/March 2016 and May/June 2018.

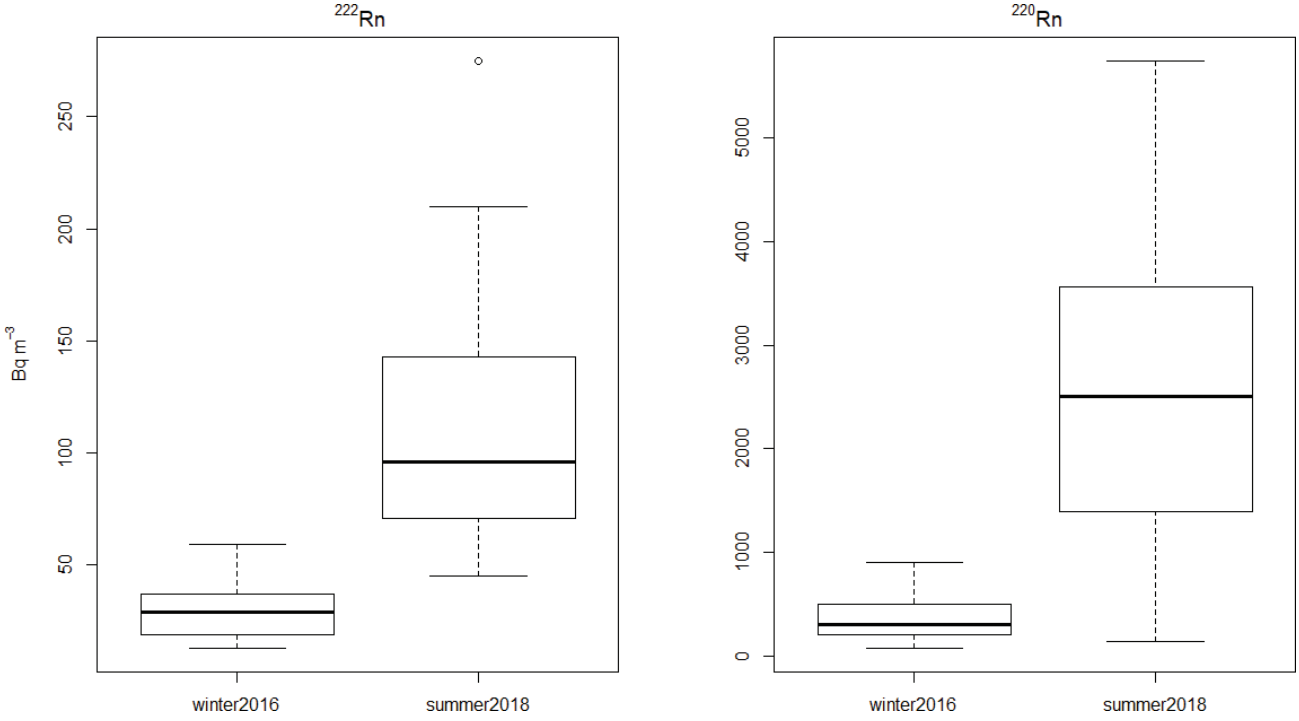

Fig. 4. Boxplot of ^{222}Rn and ^{220}Rn alpha track detector measurement results (Bq m^{-3}) during the two deployment periods. Note the different y-axis scale.

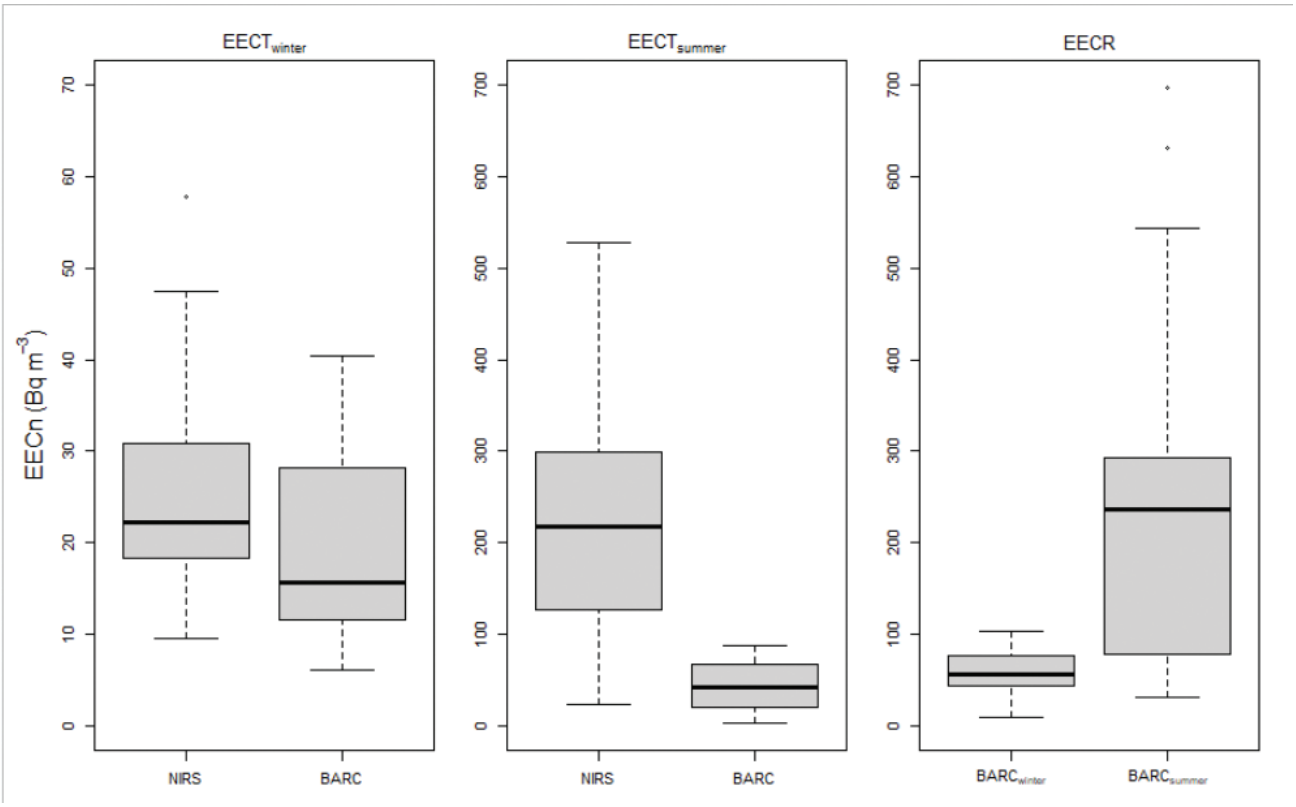

Fig. 5. Boxplot of NIRS and BARC alpha track deposition detector measurement results during the two deployment periods. Note the different y-axis scale for EECT winter.

Table 1. Summary statistics: range, median, mean, and standard deviation (SD) among localities during winter and summer deployment for alpha track detector measurements (Bq m^{-3}) of thoron (^{220}Rn), **uncorrected deposition detector measurements** of TnP (EECT), and the associated equilibrium factors (EECR/^{222}Rn) for both NIRS- and BARC-type detectors

	Winter					Summer				
	^{220}Rn	$EECT_{NIRS}$	$EECT_{BARC}$	F_{NIRS}	F_{BARC}	220Rn	$EECT_{NIRS}$	$EECT_{BARC}$	F_{NIRS}	F_{BARC}
Min	82	10	6.1	0.03	0.02	150	23	2.1	0.03	0.003
Max	910	58	42	0.27	0.02	5,700	530	87	0.18	0.07
Median	310	22	17	0.08	0.06	2,500	220	42	0.09	0.02
Mean	370	26	22	0.09	0.07	2,500	220	43	0.09	0.02
SD	210	12	12	0.06	0.05	1,400	120	25	0.04	0.02

Table 2. Summary statistics: range, median, mean, and standard deviation (SD) among localities during winter and summer deployment for alpha track detector measurements (Bq m^{-3}) of radon (^{222}Rn), **uncorrected deposition detector measurements** of RnP (EECR), and the associated equilibrium factors (EECR/^{222}Rn) for BARC-type detectors

	Winter			Summer		
	^{222}Rn	$EECR_{BARC}$	F_{BARC}	^{222}Rn	$EECR_{BARC}$	F_{BARC}
Min	13	8.6	0.32	45	31	0.43
Max	59	104	5.5	280	700	8.7
Median	29	59	1.8	96	200	2.0
Mean	31	62	2.3	110	230	2.6
SD	13	25	1.3	56	180	2.2

Citation: Journal of the European Radon Association 2021, **2**: 6130 http://dx.doi.org/10.35815/radon.v2.6130

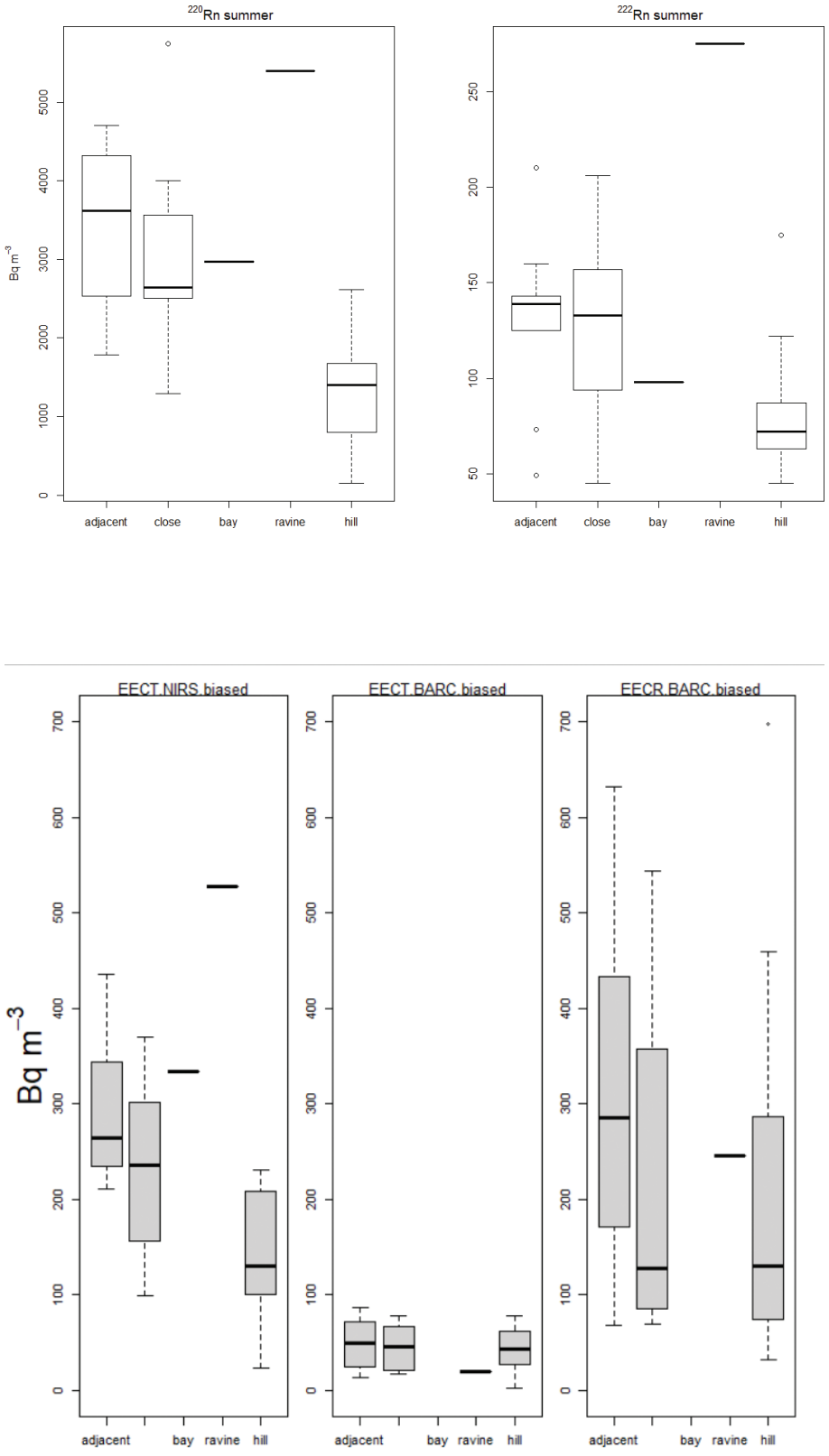

Fig. 6. Boxplots for **summer levels** of ^{220}Rn and ^{222}Rn (Bq m^{-3}) and their progeny (EECT and EECR) measured with NIRS and BARC deposition detectors adjacent (< 3 m) or close (< 20 m) to mine openings, as well as at larger distances in Fen Bay, in Mining hill and in a ravine.

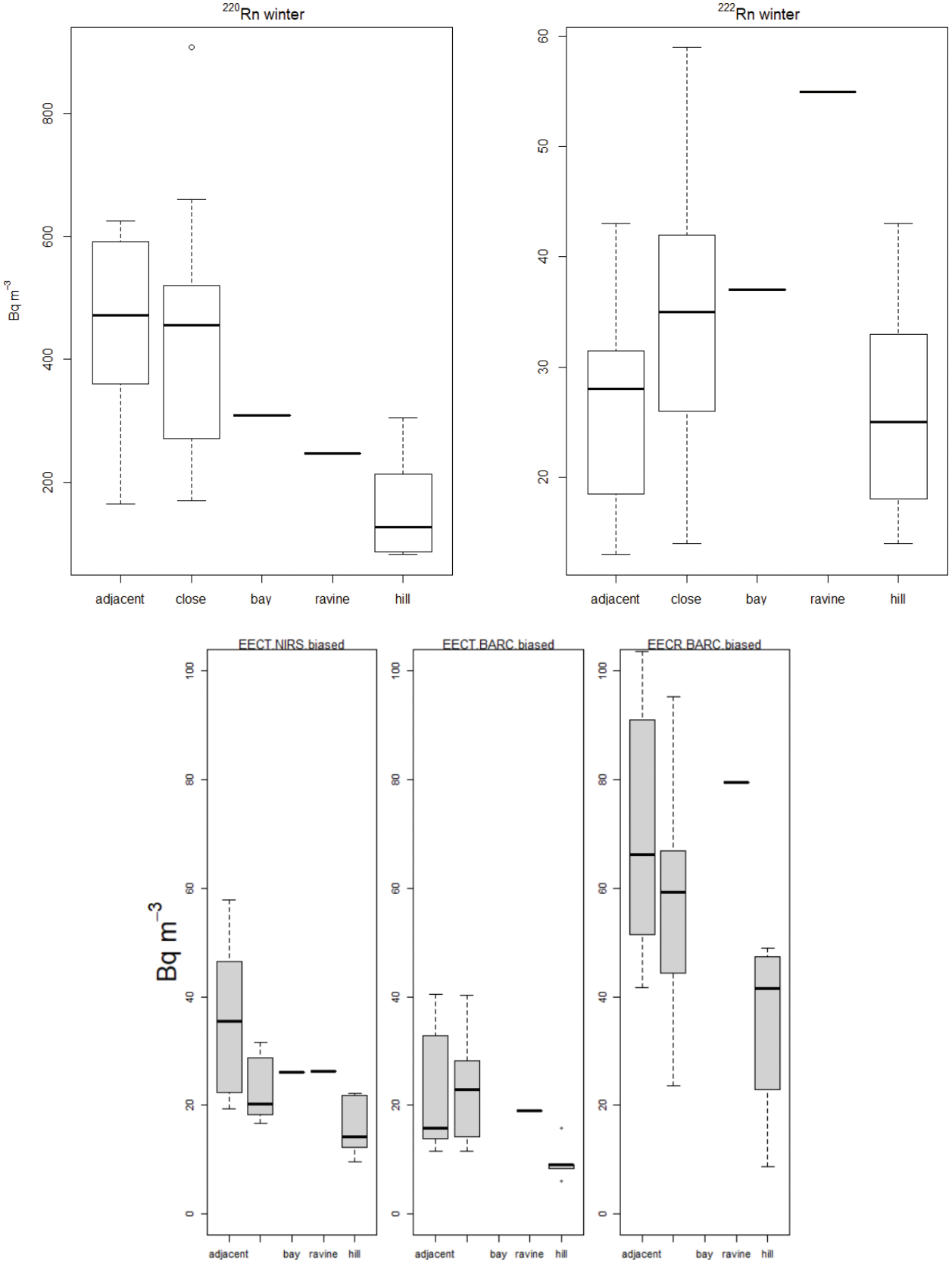

Fig. 7. Boxplots for **winter levels** of ^{220}Rn and ^{222}Rn (Bq m^{-3}) and their progeny (EECT and EECR) measured with NIRS and BARC deposition detectors adjacent (< 3 m) or close (< 20 m) to mine openings, as well as at larger distances in Fen Bay, in Mining hill and in a ravine.

Citation: Journal of the European Radon Association 2021, **2**: 6130 http://dx.doi.org/10.35815/radon.v2.6130

BARC and NIRS EECT measurements were significantly moderately correlated (Fig. 8) in both summer (r = 0.54; CI_{195}[0.21, 0.75], P < 0.01) and winter (r = 0.50; CI_{195}[0.08, 0.77], P < 0.03). However, the NIRS TnP results showed several times higher levels than the BARC TnP results (uncorrected for wind bias, Table 1). Before correcting deposition detector results for wind bias, associated equilibrium factors between progeny (EECn) and parental gas were relatively high (Tables 1 & 2). The equilibrium factor between ^{222}Rn and RnP has a global range of 0.2–0.7 with a mean of 0.5 (SD = 0.1) and a median of 0.6 (32). This suggests that the BARC RnP detectors were up to many times inflated in both summer and winter (Table 2), probably due to winds.

During the summer deployment, on the 4 days of airflow measurements, wind velocities ranged 1.1–6.1 m s^{-1} were on average 3.7 m s^{-1} (SD: 1.3), but with variation among days in wind speed but not in direction (Fig. 9). These wind velocities were significantly higher than during the rest of the summer deployment period (t = 6.3, P <

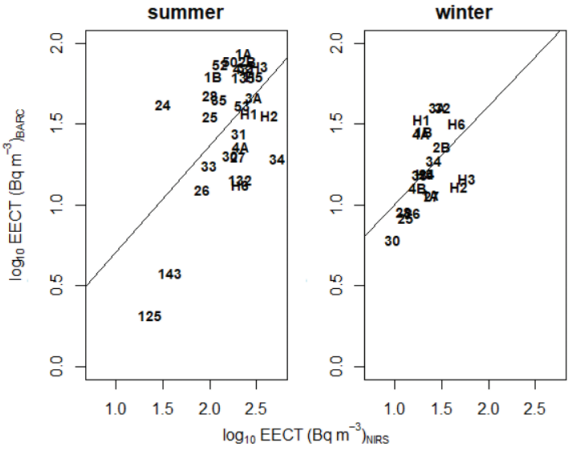

Fig. 8. Plots of correlation between EECT measured with NIRS and BARC deposition detectors during the two deployment periods. Name of locations are used rather than points.

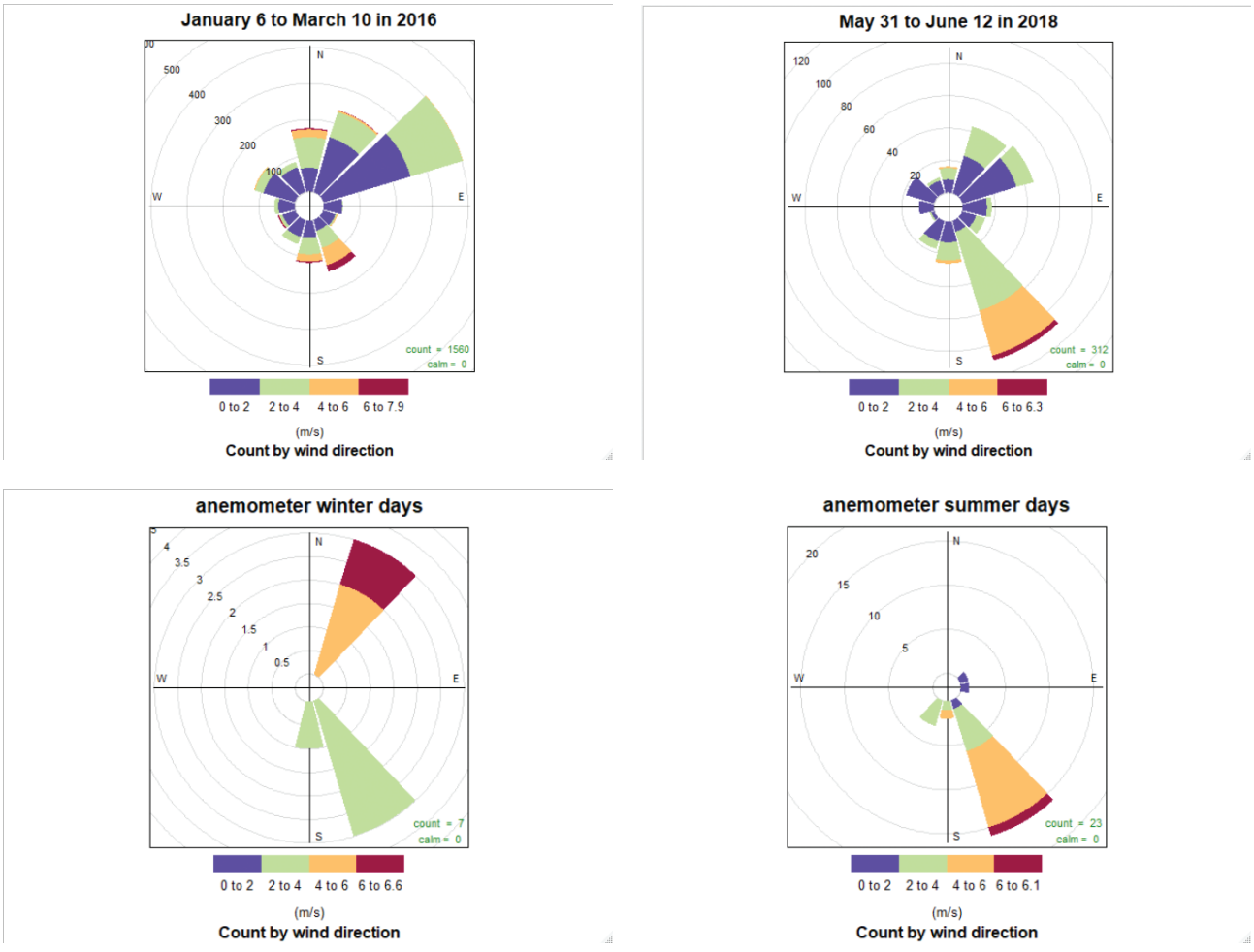

Fig. 9. Wind roses for the winter (a) and summer (b) deployment periods, and the 4 days of air-movement measurements during the summer period.

0.01), while prevailing wind direction was relatively similar (Fig. 9). The summer anemometer airflow measurements under the detector shelters ranged from 0 to 2.7 m s^{-1} (median: 0.19, mean: 0.23, and SD: 0.19) and were in a *t*-test significantly lower than concurrent wind at 10 m height (both log-transformed: $t = 170$, $P < 0.001$). Thus, airflow under detector shelters during the summer deployment period ranged from a fraction of 0.01 to 0.96 of the concurrent wind-speed (mean: 0.07 and SD: 0.03), and the mean per locality ranged from 0.03 to 0.16. This shows how well each location shelter is working. Airflow adjacent to the detector shelter ranged from 0.05 to 4.7 m s^{-1} (median: 0.8, mean: 1.0, SD: 0.8) and was in a *t*-test significantly larger than airflow velocity beneath the detector shelters (both log-transformed: $t = 34$, $P < 0.001$). Airflow beneath detector shelters in summer varied among localities and with wind strength (Fig. 10) and was explained in a linear model (adj $R^2 = 0.25$, $F(36, 2{,}797) = 28$, $P < 0.001$) by intercept ($\hat{\alpha}$: −2.6, SE: 0.08), location identity ($\hat{\beta}$ range: −3.5 to −1.9, SE < 0.2), and wind strength (log2-transformed, $\hat{\beta}$: 0.59, SE: 0.04, $t = 14$, $P < 0.01$) but not by wind direction ($\hat{\beta}$: 0, $P > 0.38$). With localities ordered according to their mean, reverse Helmert contrasts were used in the same model to show that all localities had significantly different airflow beneath detector shelters (*t* range: 2.8–13, $P < 0.01$) except three localities (*t* range: 0.8–1.7, $P > 0.08$). Variation in airflow beneath detector shelters due to location identity and varying wind speeds, thus, needs to be accounted for when assessing variation in deposition velocity of progeny of ^{220}Rn and ^{222}Rn.

During the hours of anemometer measurements on the two winter days in March 2017, wind speeds ranged from 3 to 6.6 m s^{-1} with a mean of 5 m s^{-1} (SD: 1.4). This is within the range during the 2016 winter period with detector deployment, but the average is significantly faster than in 2016 (log2-transformed: $t = 53$, $P < 0.01$). The 2 days differed from each other in both wind speed (Fig. 11) and wind direction (NNE and SSE, respectively), but both these wind directions were representative of the 2016 winter deployment period (Fig. 9). For these 2 winter days, airflow beneath shelters ranged from a fraction of 0.01–0.53 of concurrent wind speed (mean: 0.09, SD: 0.07), and among localities, the mean ranged from 0.04 to 0.25. During similar wind speeds (≥ 3 m s^{-1}), this fraction was significantly smaller in summer ($t = -13$, $P < 0.01$), while it was rather higher at lower wind speeds (Fig. 12). Locations-specific factors in winter, thus, differ from those in summer. For a comparison, the predicted airflow along detectors calculated from wind-speed during each deployment period and location-specific sheltering factors involved a strong correlation with actual anemometer measurements under summer conditions ($r = 0.88$: CI_{95}[0.77, 0.94], $P < 0.01$), but an even stronger one during winter conditions ($r = 0.96$: CI_{95}[0.92, 0.98], $P < 0.01$).

Among statistical models for biased (uncorrected) TnP or RnP deposition, the ones including predicted airflow along detectors from wind during detector deployment and location-specific sheltering factors performed equally well as the ones including anemometer airflow measurements (Table 3a). Notably, in both of these models, the airflow term did not have any effect size or significance, whereas the ^{220}Rn term was significant in all models with the clearly larger effect, and the ^{222}Rn term was significant

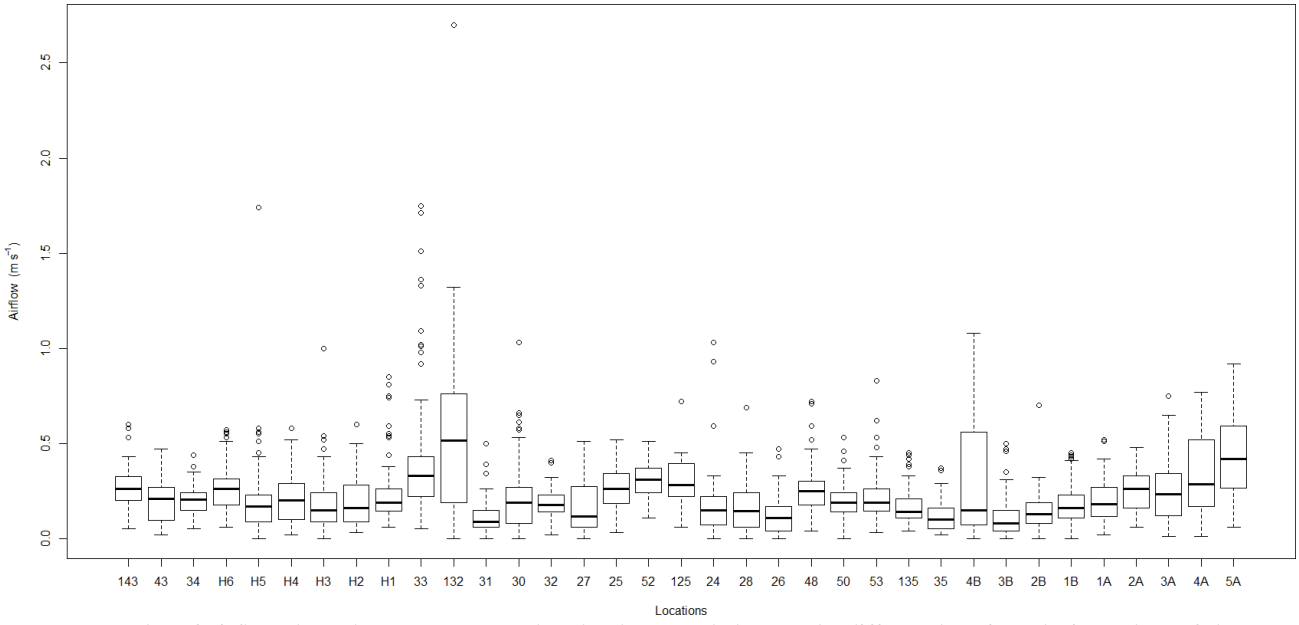

Fig. 10. Boxplot of airflow along detectors measured under detector shelters at the different locations during 4 days of the summer deployment period.

Citation: Journal of the European Radon Association 2021, **2**: 6130 http://dx.doi.org/10.35815/radon.v2.6130

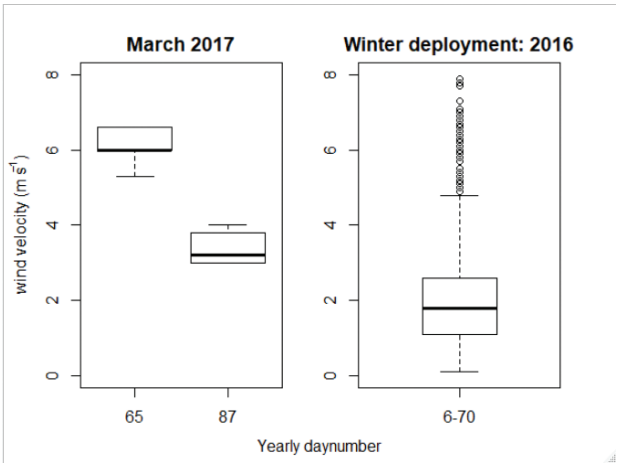

Fig. 11. Boxplot of wind speed (10 m height) during hours of airflow measurement along detectors during 2 winter days in 2017 and for the whole winter detector deployment period in 2016.

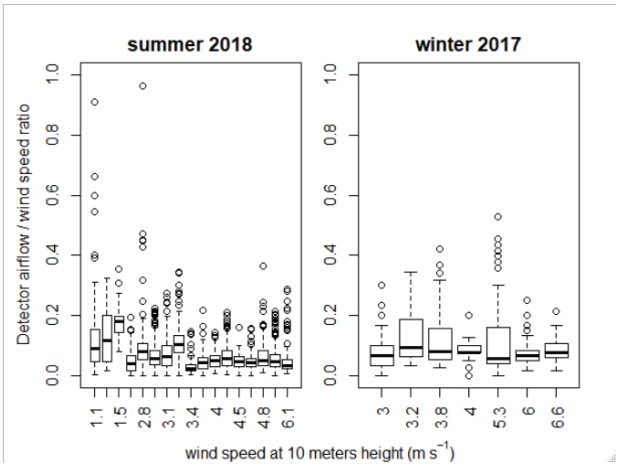

Fig. 12. Ratio between airflow along detectors beneath shelters and concurrent wind speed (10 m height) during anemometer measurements in the summer of 2018 and winter of 2017.

Table 3. Statistical models for variation in measurements of three types of deposition detectors: TnP_{NIRS}, TnP_{BARC}, and RnP_{BARC} deployed outdoors in Fen complex explained by airflow (Airfl) either (R) point measurements by anemometer or (P) predicted from average wind speed during deployment by location-specific sheltering factors, as well as levels of progenitor noble gases. Both summer and winter condition data in a) but only summer condition data used in the models in b). Akaike's Information Criterion (AIC), degrees of freedom (DF), F statistic, and adjusted R^2 for linear models explaining this variation

a)

Airfl	Model	Adj.R	F	DF	AIC
R	$\log_{10}\mathbf{TnP_{NIRS}} \sim \log_2$airflow + $\log_{10}{}^{220}$Rn + $\log_{10}{}^{222}$Rn	0.88	140	3:53	−28.8
P	$\log_{10}\mathbf{TnP_{NIRS}} \sim \log_2$predicted airflow + $\log_{10}{}^{220}$Rn + $\log_{10}{}^{222}$Rn	0.88	143	3:53	−29.7
R	$\log_{10}\mathbf{TnP_{BARC}} \sim \log_2$airflow + $\log_{10}{}^{220}$Rn + $\log_{10}{}^{222}$Rn	0.36	10	3:46	19.7
P	$\log_{10}\mathbf{TnP_{BARC}} \sim \log_2$predicted airflow + $\log_{10}{}^{220}$Rn + $\log_{10}{}^{222}$Rn	0.36	10	3:46	19.4
R	$\log_{10}\mathbf{RnP_{BARC}} \sim \log_2$airflow + $\log_{10}{}^{220}$Rn + $\log_{10}{}^{222}$Rn	0.49	16	3:45	26.2
P	$\log_{10}\mathbf{RnP_{BARC}} \sim \log_2$predicted airflow + $\log_{10}{}^{220}$Rn + $\log_{10}{}^{222}$Rn	0.48	16	3:45	26.4

b)

Airfl	Model	Adj.R	F	DF	AIC
R	$\log_{10}TnP_{NIRS} \sim \log_2$airflow + $\log_{10}{}^{220}$Rn + $\log_{10}{}^{222}$Rn	0.70	26	3:29	−12.0
P	$\log_{10}TnP_{NIRS} \sim \log_2$predicted airflow + $\log_{10}{}^{220}$Rn + $\log_{10}{}^{222}$Rn	0.70	26	3:29	−11.8
R	$\log_{10}TnP_{BARC} \sim \log_2$airflow + $\log_{10}{}^{220}$Rn + $\log_{10}{}^{222}$Rn	0.45	9	3:26	9.6
P	$\log_{10}TnP_{BARC} \sim \log_2$predicted airflow + $\log_{10}{}^{220}$Rn + $\log_{10}{}^{222}$Rn	0.49	10	3:26	7.5
R	$\log_{10}RnP_{BARC} \sim \log_2$airflow + $\log_{10}{}^{220}$Rn + $\log_{10}{}^{222}$Rn	0.15	3	3:26	25.2
P	$\log_{10}RnP_{BARC} \sim \log_2$predicted airflow + $\log_{10}{}^{220}$Rn + $\log_{10}{}^{222}$Rn	0.13	3	3:26	26

in the two NIRS models (Table 4a). However, given the known effect, bias of airflow on deposition velocities (14, 16–18), and the much higher levels of airborne radionuclides observed under summer conditions than winter conditions in Fen complex, we ran the same statistical models with only the summer data. This involved slightly different model performances (Table 3b), and in the models for BARC TnP detectors, the airflow term was highly significant (Table 4b). Notably for all these models, the significant ^{220}Rn term had an even larger effect, and for the BARC

Table 4. Parameter estimates (SE) and their significance (*) of explanatory variables in linear models of variation in measurements of three types of deposition detectors: TnPNIRS, TnPBARC, and RnPBARC deployed outdoors in Fen complex. Explanatory variables are for β1 either R) point measurements of airflow by anemometer or P) airflow predicted from average wind speed during deployment by location-specific sheltering factors, in addition to ^{220}Rn and ^{222}Rn progenitor noble gases. Both summer and winter condition data in a) but only summer condition data used in the models in b)

a)

Type: Y ~	α: intercept	β_1: $\log_2$**R** or $\log_2$**P**	β_2:$\log_{10}$ ^{220}Rn	β_2: $\log_{10}$ ^{222}Rn
R: $\log_{10}$TnP$_{NIRS}$	−0.93 (.14) *	−0.01 (.06)	0.68 (.08) *	0.43 (.12) *
P: $\log_{10}$TnP$_{NIRS}$	−0.86 (.16) *	0.05 (.06)	0.68 (.08) *	0.47 (.12) *
R: $\log_{10}$TnP$_{BARC}$	0.21 (.24)	−0.09 (.10)	0.57 (.14) *	−0.34 (.20)
P: $\log_{10}$TnP$_{BARC}$	0.06 (.27)	−0.10 (.10)	0.60 (.14) *	−0.34 (.20)
R: $\log_{10}$RnP$_{BARC}$	0.21 (.27)	0.10 (.11)	0.62 (.15) *	0.06 (.21)
P: $\log_{10}$RnP$_{BARC}$	0.35 (.32)	0.09 (.11)	0.59 (.15) *	0.05 (.26)

b)

Type:Y ~	α: intercept	β_1: $\log_2$**R** or $\log_2$**P**	β_2:$\log_{10}$ ^{220}Rn	β_2: $\log_{10}$ ^{222}Rn
R: $\log_{10}$TnP$_{NIRS}$	−0.71 (.35)	−0.08 (.08)	0.68 (.11) *	0.29 (.16)
P: $\log_{10}$TnP$_{NIRS}$	−0.69 (.38)	−0.05 (.07)	0.69 (.11) *	0.29 (.16)
R: $\log_{10}$TnP$_{BARC}$	−0.18 (.57)	−0.39 (.14) *	0.83 (.18) *	−0.79 (.26) *
P: $\log_{10}$TnP$_{BARC}$	−0.52 (.59)	−0.39 (.12) *	0.93 (.17) *	−0.89 (.25) *
R: $\log_{10}$RnP$_{BARC}$	1.10 (.74)	0.17 (.18)	0.55 (.23) *	−0.20 (.33)
P: $\log_{10}$RnP$_{BARC}$	1.02 (.80)	0.08 (.16)	0.55 (.24) *	−0.20 (.35)

TnP detector models, the ^{222}Rn term was also significant but with a negative effect. Among the two BARC TnP detector models, the one with airflow along detectors predicted from wind during the whole deployment period performed slightly better than the model with airflow measured with anemometer (Table 3b). This can be explained by the lower average wind speed during deployment compared with during anemometer measurements. Interestingly, the only model term being significant in the BARC RnP models was the ^{220}Rn term (positive relation).

For the BARC detectors, correction of wind bias using the anemometer airflow measurements without accounting for different wind speeds during the whole deployment period involves even significantly lower estimates of both TnP ($t = -2.8$, $P < 0.01$) and RnP ($t = -2.5$, $P < 0.02$). This justifies the effort in establishing location-specific sheltering factors to provide better predictions of airflow along detectors, integrated for the whole detector deployment period. Wind bias on BARC deposition detectors was, thus, corrected for by using the predicted location-specific airflow along detectors during the whole deployment periods (see methods) rather than anemometer measurements. This resulted in relatively realistic outdoor ^{222}Rn to progeny equilibrium factors (Table 5). The magnitude of wind bias when accounting for this predicted airflow from location-specific sheltering factors was large and constituted a fraction of the total TnP detector measurement (biased) ranging from 0.74 to 0.96 (mean: 0.87, SD: 5). In other words, the fraction of the BARC TnP deposition detector measurement remaining after correcting for wind bias ranged from 0.04 to 0.26 (mean: 0.13, SD: 0.05). By comparison, the corresponding wind bias fraction predicted by the airflow term in the most likely statistical model (BARC TnP) ranged from 2 to 82 (mean: 11, SD: 13), and this model predicted TnP activity concentrations ranging from 3 to 69 Bq m^{-3} (mean: 29, SD: 17) when plugging in location-specific predicted airflow values and observed ^{220}Rn and ^{222}Rn measurements.

Discussion

Despite the significant sheltering effect of detector shelters, wind bias was obvious in the uncorrected results from both NIRS and BARC deposition detectors (Tables 1 & 2), and from the many times inflated equilibrium factor (F) for ^{222}Rn compared to global outdoor ranges (1, 2). Bias from airflow velocities as low as 0.1 and 0.2 m s^{-1} has, thus, been shown for indoor conditions (18). By establishing knowledge on how alpha deposition detectors are biased by outdoor winds, uncertainties in outdoors exposure can be reduced. This is especially true for ^{220}Rn and progenies, since TnP measurements should be used for dosimetry due to large uncertainties in their equilibrium factor with ^{220}Rn (10–13). The way we have corrected for wind bias using location-specific prediction of airflow

Citation: Journal of the European Radon Association 2021, **2**: 6130 http://dx.doi.org/10.35815/radon.v2.6130

Table 5. Summary statistics: range, median, mean, and standard deviation (SD) among localities for winter and summer BARC TnP (EECT) and RnP (EECR) deposition detector measurements **corrected for wind bias** (predicted per locality from wind speed during deployment and location-specific sheltering factors from ratio between anemometer airflow along detectors and concurrent wind speed), and the associated equilibrium factors

	Winter				Summer			
	$EECT_{BARC}$	$EECR_{BARC}$	F_{EECT}	F_{EECR}	$EECT_{BARC}$	$EECR_{BARC}$	F_{EECT}	F_{EECR}
Min	0.3	0.6	0.002	0.02	0.2	2.6	0.001	0.05
Max	5.2	14	0.016	0.71	18	76	0.01	1.2
Median	1.9	6.3	0.006	0.23	6.7	27	0.003	0.26
Mean	2.1	6.7	0.007	0.26	6.4	31	0.004	0.36
SD	1.2	2.9	0.004	0.15	4.3	22	0.003	0.31

along detectors seems to give realistic outdoor values for the equilibrium (F) of ^{222}Rn and RnP, giving support to these results. However, variation is relatively large, probably reflecting variation among localities in successfully predicting airflow and associated uncertainties, which only can be reduced by assessing more anemometer and weather data. When we used location-specific sheltering factors and wind conditions during the whole deployment periods to correct for wind bias on BARC TnP results, the bias constituted a smaller fraction than when using actual anemometer measurements on days with a higher wind speed than the deployment period wind speed average. An even smaller magnitude of wind bias was predicted by the most likely statistical model. This suggests that the wind bias correction using location-specific sheltering factors is conservative.

The outdoor TnP and RnP levels estimated from deposition detectors after correcting for predicted airflow bias were 4–26% as large as the biased estimates, showing the importance of taking wind-bias into account. The statistical models show the importance of accounting for location-specific sheltering and winds during the whole deployment period, and not just using single anemometer measurements. We, thus, show the importance of establishing location-specific sheltering factors that express the ratio between airflow along the detector and concurrent wind speed, to be able to predict airflow along each detector from the wind prevailing during deployment. During the summer deployment period of this investigation, which involved the most significant levels of progeny, wind directions did not involve much variation. Most likely, location-specific sheltering factors should for any deployment period also include the effect of any different wind directions, which probably should be assessed each time deposition detectors are applied outdoors.

In the investigated Mining hill area, outdoor levels of radionuclides in the air are significantly higher than global averages, which, for example, are around 10 Bq m^{-3} for ^{220}Rn and ^{222}Rn (1, 2). This is due to the surfacing redrock and soil in the investigated area (6, 8) and, in particular, because of mine ventilation (5, 22). This is in line with other investigations of NORM (4). Airborne radionuclide levels in this investigation show large seasonal variation, with the generally low levels observed in winter being related to reduced exhalation because of snow and ice cover and the few high local levels in winter relating to ventilating mine openings. This is supported by the fact that equilibrium values (F) are much more inflated at localities adjacent to mine openings.

The NIRS depostion detector results were not wind corrected due to the very different results on wind bias compared to the BARC detectors. A higher sensitivity of the NIRS CR-39 detectors compared to BARC LR-115 detectors involves more tracks per square centimeter (33), but detector materials can be sensitive to temperature, like demonstrated for CR-39, where the sensitivity of detectors decreases with temperature (34, 35). A different temperature sensitivity between NIRS and BARC detectors could help explain that the NIRS TnP results showed much higher summer levels than the BARC TnP results (uncorrected). Moreover, recent results from an underground mine with airflow velocities altering between 0.1–0.3 m s^{-1} and 0.3–0.5 m s^{-1} showed TnP levels measured with these NIRS detectors that were equal to an in-situ instrument measurements, even though it should be noted that the instrument uncertainty could involve up to twice as large real values (36).

The results of the study at hand should be verified through repeated in-situ measurments during similar temperatures and weather conditions as during detector deployment. The inaccuracies of using wind data from a weather station 1,100 m away should be reduced by modeling wind speed and direction at each location. More anemomemeter data from each location and concurrent wind speeds and directions at the weather station should be made to model wind at Fen compared to at the weather station. Also, a calibration curve assessing bias from airflow at different speeds should be established in a thoron room with known activity concentrations, possibly with different fractions of attached and unattached progeny.

This should be done for both NIRS and BARC detectors. Due to smaller mass and electric charge, unattached progenies have deposition velocities up to 100 times faster than attached progeny, which would be important both to seasonal measurements with or without foliage and help reduce uncertainties in subsequent dose rates.

Conclusions

Relatively high levels of TnP have been measured with time integrating alpha track deposition detectors in outdoor air at Mining hill in Fen complex, but bias from airflow on deposition velocities involves high uncertainties. This has been addressed in the study at hand. Our initial correction of the bias used actual airflow measurements beneath detector shelters on a few of the detector deployment days and involved a relatively large estimated bias with still much uncertainty. During the whole detector deployment period, the average airflow beneath shelters from outdoor winds was actually much lower than what was measured on the few measurement days. When we assessed variation in airflow under detector shelters and covariation in weather parameters to identify location-specific factors of wind reduction, we were able to more precisely predict airflow for the whole detector deployment period. This involved a lower estimated bias from airflow for the BARC detectors and lower uncertainties. An even lower bias was estimated when taking into account a statistical model assessing variation in BARC TnP detectors together with covariation in ambient radon and thoron levels together with the predicted airflow.

Acknowledgments

This work was (partly) supported by the Research Council of Norway through its Centres of Excellence funding scheme, project number 223268/F50. This was received through the Centre for Environmental Radioactivity, CERAD, and Centre of Excellence, CoE. We thank the Norwegian Meteorological Institute (MET) for access to and being allowed to download weather data from www.eklima.no. We also thank for the help with fieldwork Ingvild Engen Finne at DSA, as well as Ester Netland Simonsen and Atle Ørbeck Hansen.

Conflict of interest and funding

The authors have not received any funding or benefits from industry or elsewhere to conduct this study.

References

1. UNSCEAR. Sources and effects of ionizing radiation. Volume I: sources. Annex B: Exposures from natural radiation sources. UNSCEAR report to the General Assembly, with annexes. New York, NY: United Nations Scientific Committee on the Effect of Atomic Radiation; 2000.
2. UNSCEAR. Effects of ionizing radiation. Volume II, Annex E: Sources-to-effects assessment for radon in homes and workplaces. UNSCEAR report to the General Assembly, with annexes. New York, NY: United Nations Scientific Committee on the Effect of Atomic Radiation; 2006.
3. Ramola RC, Gusain GS, Rautela BS, Sagar DV, Prasad G, Shahoo SK, et al. Levels of thoron and progeny in high background radiation area of southeastern coast of Odisha, India. Radiat Protect Dosim 2012; 152(1–3): 62–5. doi: 10.1093/rpd/ncs188
4. Ishimori Y, Lange K, Martin P, Mayya YS, Phaneuf M. Measurement and calculation of radon releases from NORM residues. 2013. Technical reports series no. 474, ISSN 0074–1914, Vienna: International Atomic Energy Agency, 2013.
5. Haanes H, Finne IE, Kolstad T, Mauring A, Dahlgren S, Rudjord AL. Outdoor thoron and progeny in a thorium rich area with old decommissioned mines and waste rock. J Environ Radioact 2016; 10(162–163): 23–32. doi: 10.1016/j.jenvrad.2016.05.005
6. Popic JM, Bhatt CR, Salbu B, Skipperud L. Outdoor 220Rn, 222Rn and terrestrial gamma radiation levels: investigation study in the thorium rich Fen Complex, Norway. J Environ Monit 2012; 14(1): 193–201. doi: 10.1039/C1EM10726G
7. Stranden E. Thoron (220Rn) daughter to radon (222Rn) daughter ratios in thorium-rich areas. Health Physics 1984; 47(5): 784–5.
8. Stranden E. The radiological impact of mining in a Th-rich Norwegian area. Health Physics 1985; 48(4): 415–20. doi: 10.1097/00004032-198504000-00003
9. Meisenberg O, Tschiersch J. Thoron in indoor air: modeling for a better exposure estimate. Indoor Air 2011; 21(3): 240–52. doi: 10.1111/j.1600-0668.2010.00697.x
10. Bangotra P, Mehra R, Kaur K, Kanse S, Mishra R, Sahoo BK. Estimation of EEC, unattached fraction and equilibrium factor for the assessment of radiological dose using pin-hole cup dosimeters and deposition based progeny sensors. J Environ Radioactiv 2015; 148(0): 67–73. doi: 10.1016/j.jenvrad.2015.06.010
11. Janik M, Tokonami S, Kranrod C, Sorimachi A, Ishikawa T, Hosoda M, et al. Comparative analysis of radon, thoron and thoron progeny concentration measurements. J Radiat Res Appl Sci 2013; 54(4): 597–610. doi: 10.1093/jrr/rrs129
12. Mayya YS, Mishra R, Prajith R, Gole AC, Sapra BK, Chougaonkar MP, et al. Deposition-based passive monitors for assigning radon, thoron inhalation doses for epidemiological studies. Radiat Protect Dosim 2012; 152(1–3): 18–24. doi: 10.1093/rpd/ncs196
13. Mishra R, Mayya YS. Study of a deposition-based direct thoron progeny sensor (DTPS) technique for estimating equilibrium equivalent thoron concentration (EETC) in indoor environment. Radiat Meas 2008; 43(8): 1408–16. doi: 10.1016/j.radmeas.2008.03.002
14. Porstendörfer J. Properties and behaviour of radon and thoron and their decay products in the air. J Aerosol Sci 1994; 25(2): 219–63. doi: 10.1016/0021-8502(94)90077-9
15. Zhuo W, Iida T. Estimation of thoron progeny concentrations in dwellings with their deposition rate measurements. Japanese J Health Phys 2000; 35(3): 365–70. doi: 10.5453/jhps.35.365
16. Mishra R, Prajith R, Sapra BK, Mayya YS. Response of direct thoron progeny sensors (DTPS) to various aerosol concentrations and ventilation rates. Nuclear instruments and methods in physics research section B: beam interactions with materials and atoms. Sci Direct 2010; 268(6): 671–5. doi: 10.1016/j.nimb.2009.12.012

17. Lai ACK, Nazaroff WW. Modelling indoor particle deposition from turbulent flow into smooth surfaces. J Aerosol Sci 2000; 31(4): 463–76. doi: 10.1016/S0021-8502(99)00536-4
18. Mishra R, Prajith R, Rout RP, Sriamirullah J, Sapra BK. Effect of air velocity on inhalation doses due to radon and thoron progeny in a test chamber. Radiat Protect Dosim 2020; 189(3): 401–5. doi: 10.1093/rpd/ncaa054
19. Andersen T. Secondary processes in carbonatites: petrology of "rødberg" (hematite-calcite-dolomite carbonatite) in the Fen central complex, Telemark (South Norway). Lithos 1984; 17(0): 227–45. doi: 10.1016/0024-4937(84)90022-7
20. Brøgger WC. Die eruptivgesteine des Kristianiagebietes. IV. Fangebiet in Telemark, Norwegen. 1921. Norske skrifter udgit av (published by) Videnskapsselskabet i (in) Kristiania 1921; I. Math. Nat. Klasse. No. 9:1–408.
21. Dahlgren S. Fenfeltet – et stykke eksplosiv geologi. (in Norwegian). Stein, magasin for populærgeologi 1993; 144–5.
22. Haanes H, Rudjord AL. Significance of seasonal outdoor releases of thoron from airflow through a point source during natural ventilation of a mine-complex in thorium-rich bedrock. Atmos Pollut Res 2018; 9(6): 1000–8. doi: 10.1016/j.apr.2018.03.007
23. Mishra R, Prajith R, Sapra BK, Mayya YS. An integrated approach for the assessment of the thoron progeny exposures using direct thoron progeny sensors. Radiat Prot Dosim 2010; 141(4): 363–6. doi: 10.1093/rpd/ncq236
24. Mayya YS, Mishra R, Prajith R, Sapra BK, Kushwaha HS. Wire-mesh capped deposition sensors: novel passive tool for coarse fraction flux estimation of radon thoron progeny in indoor environments. Sci Total Environ 2010; 409(2): 378–83. doi: 10.1016/j.scitotenv.2010.10.007
25. Mishra R, Rout R, Prajith R, Jalalluddin S, Sapra BK, Mayya YS. Innovative easy-to-use passive technique for 222RN and 220RN decay product detection. Radiat Protect Dosim 2016; 171(2): 181–186. doi: 10.1093/rpd/ncw053
26. Roupsard P, Amielh M, Maro D, Coppalle A, Branger H, Connan O, et al. Measurement in a wind tunnel of dry deposition velocities of submicron aerosol with associated turbulence onto rough and smooth urban surfaces. J Aerosol Sci 2013; 55: 12–24. doi: 10.1016/j.jaerosci.2012.07.006
27. Aalto P, Hameri K, Paatero P, Kulmala M, Bellander T, Berglind N, et al. Aerosol particle number concentration measurements in five European cities using TSI-3022 condensation particle counter over a three-year period during health effects of air pollution on susceptible subpopulations. J Air Waste Manag Assoc 2005; 55(8): 1064–76. doi: 10.1080/10473289.2005.10464702
28. R Core Team. R: a language and environment for statistical computing. 2020 (version 4.0.2, June 2020), In: Computing RFfS, editor. Vienna, Austria. Available from: https://www.R-project.org/.
29. Pebesma EJ, Bivand RS. Classes and methods for spatial data in R. R News 2005; 5(2): 9–13.
30. Bivand R, Keitt T, Rowlingson B. Rgdal: Bindings for the 'Geospatial' data abstractation library. R package version 1.4–4. 2019 (cited and used June 2020). Available from: https://CRAN.R-project.org/package=rgdal
31. Carslaw DC, Ropkins K. Openair – an R package for air quality data analysis. Environ Model Software 2012; 27–28: 52–61. doi: 10.1016/j.envsoft.2011.09.008
32. Chen J, Harley NH. A review of indoor and outdoor radon equilibrium factors-part I: 222Rn. Health Phys 2018; 115(4): 490–9. doi: 10.1097/HP.0000000000000909
33. Nikolaev VA, Ilić R. Etched track radiometers in radon measurements: a review. Radiat Meas 1999; 30(1): 1–13. doi: 10.1016/S1350-4487(98)00086-9
34. O'Sullivan D, Thompson A, Adams JA, Beahm LP. New results on the investigation of the variation of nuclear track detector response with temperature. Nucl Tracks Radiat Meas 1984; 8(1): 143–6. doi: 10.1016/0735-245X(84)90074-7
35. Kodaira S, Yasuda N, Tawara H, Ogura K, Doke T, Hasebe N, et al. Temperature and pressure conditions for the appropriate performance of charge and mass resolutions in balloon-borne CR–39 track detector for the heavy cosmic rays. Nuclear instruments and methods in physics research section B: beam interactions with materials and atoms. Sci Direct 2009; 267(10): 1817–22. doi: 10.1016/j.nimb.2009.03.001
36. Kleinschmidt R, Watson D, Janik M, Gillmore G. The presence and dosimetry of radon and thoron in a historical, underground metalliferous mine. J Sustain Min 2018; 17(3): 120–30. doi: 10.1016/j.jsm.2018.06.003

***Hallvard Haanes**
Norwegian Radiation and Nuclear Safety Authority,
Grini Næringspark 13, 1361 Østerås,
Norway
Email: Hallvard.Haanes@dsa.no